ACS Chemical Neuroscience

pubs.acs.org/chemneuro Research Article

APPI-Derived Cyclic Peptide Enhances Aβ42 Aggregation and Reduces Aβ42-Mediated Membrane Destabilization and Cytotoxicity

Shiran Lacham-Hartman, Reut Moshe, Shani Ben-Zichri, Yulia Shmidov, Ronit Bitton, Raz Jelinek, and Niv Papo*

Cite This: https://doi.org/10.1021/acschemneuro.3c00208 Read Online

ACCESS | Metrics & More | Article Recommendations | Supporting Information

ABSTRACT: An amyloid precursor protein inhibitor (APPI) and amyloid beta 42 (Aβ42) are both subdomains of the human transmembrane amyloid precursor protein (APP). In the brains of patients with Alzheimer's disease (AD), Aβ42 oligomerizes into aggregates of various sizes, with intermediate, low-molecular-weight Aβ42 oligomers currently being held to be the species responsible for the most neurotoxic effects associated with the disease. Strategies to ameliorate the toxicity of these intermediate Aβ42 oligomeric species include the use of short, Aβ42-interacting peptides that either inhibit the formation of the Aβ42 oligomeric species or promote their conversion to high-molecular-weight aggregates. We therefore designed such an Aβ42-interacting peptide that is based on the β-hairpin amino acid sequence of the APPI, which exhibits high similarity to the β-sheet-like aggregation site of Aβ42. Upon tight binding of this 20-mer cyclic peptide to Aβ42 (in a 1:1 molar ratio), the formation of Aβ42 aggregates was enhanced, and consequently, Aβ42-mediated cell toxicity was ameliorated. We showed that in the presence of the cyclic peptide, interactions of Aβ42 with both plasma and mitochondrial membranes and with phospholipid vesicles that mimic these membranes were inhibited. Specifically, the cyclic peptide inhibited Aβ42-mediated mitochondrial membrane depolarization and reduced Aβ42-mediated apoptosis and cell death. We suggest that the cyclic peptide modulates Aβ42 aggregation by enhancing the formation of large aggregates—as opposed to low-molecular-weight intermediates—and as such has the potential for further development as an AD therapeutic.

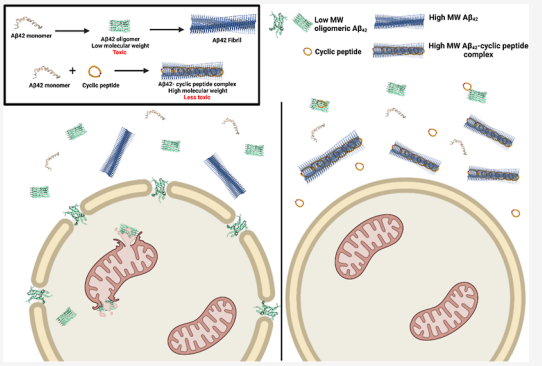

KEYWORDS: *APPI, Aβ42, Alzheimer's disease, artificial membranes, neuronal cell toxicity, peptide−lipid interactions*

INTRODUCTION

Alzheimer's disease (AD)—the most prevalent neurodegenerative disease—is characterized by memory impairment and loss of neuronal function. It is commonly held that AD is associated with the accumulation of intra- and extracellular amyloid beta (Aβ) plaques formed as a result of proteolysis of the amyloid precursor protein (APP) by overexpressed β- and γ-secretases.[1,2] APP is a type I transmembrane glycoprotein that is abundantly expressed in the mitochondrial and cell membranes of mammals.[3,4] As a result of alternative splicing, three major isoforms of APP are produced, namely, APP695, APP751, and APP770 (ranging in size between 110 and 140 kDa).[5,6] The latter two isoforms contain a 58-amino-acid residue, known as the amyloid precursor protein inhibitor (APPI) [or the Kunitz protease inhibitor domain (KPI)], in the N-terminus of the extracellular region, whereas APP695 lacks this subdomain.[7] Of note, in healthy individuals, APP695 is predominantly expressed in the brain, and APP751 and APP770, in the kidneys, lungs, and heart, but in AD patients, APP751 and APP770 levels increase in brain tissue.[8−10] However, neither the implications of the expression patterns and tissue distribution of the different alternative splicing products nor the role played by the APPI in neurotoxicity is known, despite the huge body of work on the pathology of AD.

It is nonetheless known that APP proteolysis (i.e., amyloidogenic processing) occurs in pathological conditions such as AD. Sequential cleavage of the APP C-terminus by β- and γ-secretases generates multiple Aβ fragments. In particular, research over the past few decades has generated evidence that one of these fragments, Aβ42, spontaneously forms low-molecular-weight oligomeric aggregates (in the 11−19 kDa range) in solution,[11−15] thereby facilitating the subsequent formation of the high-molecular-weight amyloid aggregates, such as the fibrils and plaques, which have been associated with AD. However, the notion that Aβ42 fibrils and/or plaques are the species that cause toxicity and neurodegeneration has changed as AD research has progressed: whereas initial studies

Received: March 30, 2023
Accepted: July 31, 2023

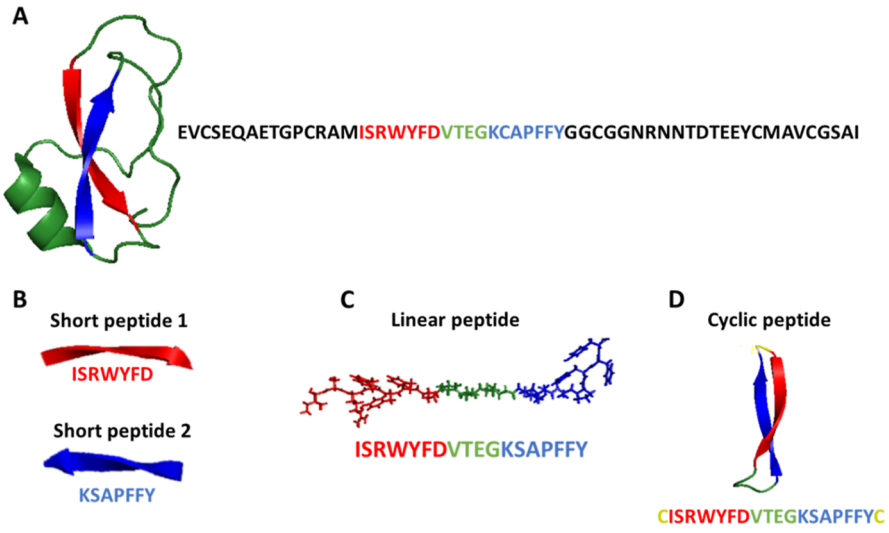

Figure 1. β-Sheet peptide fragments derived from the APPI scaffold. (A) Cartoon representation of the crystal structure (PDB: 3L33) and one-letter code sequence of the APPI. (B) Short peptide fragments representing the β-hairpin region of the APPI and their one-letter code sequences. (C) Linear peptide harboring the two β strands that originate from the β-hairpin structure in the full-length APPI scaffold. (D) Cyclic peptide similar to the linear peptide in (C), but containing cysteine residues (marked in yellow) at the N- and C-termini of the sequence; the cysteines form a disulfide bridge to mimic the β-hairpin structure in the APPI scaffold. The blue and red letters represent the β strands in the APPI structure. The green letters designate a peptide with a random structure connecting the two strands in the wild-type structure of the APPI.

postulated amyloid fibrils to be the cause of cell death and disease pathogenesis,[16] recent studies suggest that intermediate low-molecular-weight oligomeric Aβ42 species, but not high-molecular-weight Aβ aggregates, such as fibrils, are probably the most toxic species.[17,18]

Aβ42, which is predominantly generated extracellularly via proteolytic processing of APP (located in the plasma membrane and extending into the extracellular matrix), is internalized into neuronal cells via several mechanisms. These mechanisms may include active transport of Aβ42 via proteins, such as the low-density lipoprotein receptor-related protein 1 (LRP-1) and α7 nicotinic acetylcholine receptors,[19,20] or direct interaction of Aβ42 with membrane phospholipids, resulting in the formation of pores through which Aβ42 species are internalized into cells.[21,22] For example, Tahara et al. reported that cells of the BV-2 mouse microglial line treated with 1 μM extracellular Aβ42 showed an ~50% decrease in Aβ42 concentration in the extracellular medium after 24 h due to internalization into the cells.[23] This concept of a relationship between neurotoxicity and Aβ42 aggregation and internalization into cells was then demonstrated for Aβ42 monomers, oligomers, and fibrils. For example, Jin et al. showed that Aβ42 oligomers in low nanomolar concentrations were internalized into SH-EP neuroblastoma cells, where they inhibited mitochondrial activity, whereas monomeric Aβ42 at high nanomolar concentrations was inefficiently internalized into the cells.[24] The study by Ahmed et al. showed that Aβ42 fibrils were less toxic to mitochondrial activity than Aβ42 oligomers, as evaluated by an MTT assay.[25] However, despite these and many other studies on the mechanism and consequences of Aβ42 aggregation, the exact mechanism of the neurotoxicity of Aβ42 and the relationship between neurotoxicity and Aβ42 aggregation are still not fully understood. Numerous studies have nevertheless shown that following interaction with plasma and mitochondrial phospholipid membranes, low-molecular-weight oligomeric Aβ42 intermediates[25−27] disrupt membrane integrity by generating pores that allow uncontrolled transmembrane flux of small molecules, such as Ca^{2+} ions, and penetration of Aβ42 oligomers into the cell, where they subsequently accumulate.[28−31] The intracellular accumulation of Aβ42 oligomers has been demonstrated to cause mitochondrial function impairment through the disruption of respiratory chain activity, leading to apoptosis of neuronal cells.[32]

On the basis of the research done to date, our working hypothesis for this study was that intermediate low-molecular-weight Aβ42 oligomers are more toxic than the higher molecular weight Aβ42 fibrils. We therefore aimed to produce an Aβ42-interacting short peptide that would either inhibit the formation of the low-molecular-weight Aβ42 oligomeric species or promote their conversion to high-molecular-weight fibrils. This idea was based on previous studies that have shown that short peptides harboring Aβ hydrophobic motifs can be used for modulating Aβ42 aggregation and hence for preventing Aβ42-mediated neurotoxicity. Many studies have indeed designed peptides with the ability to inhibit the formation of oligomeric Aβ42 species,[33,34] and several studies have designed peptides that enhance the formation of high-molecular-weight Aβ42 aggregates (i.e., fibrils).[35−37] For example, Sun et al. showed that treatment of Aβ42 with short peptides containing an EIVY motif enhanced the formation of Aβ42 fibrils in comparison to untreated Aβ42. Those authors suggested that the EIVY-containing peptides interfered with Aβ42 oligomerization and thus reduced Aβ42-mediated cytotoxicity in mouse neuroblastoma cells.[36] The translational thread of that research was, however, not continued, as those peptides were not suitable for therapeutic application by virtue of their being effective only at high peptide to Aβ42 molar ratios and by virtue of the lack of data on their ability to self-aggregate. We note that similar strategies have been used to inhibit the toxicity of amylin or IAPP in type-2 diabetes.[38,39] In the current study, we posited that short peptides derived from the β-hairpin region within the APPI would interact with Aβ42 (also located in the APP sequence) through hydrophobic interactions resembling those producing Aβ42 aggregates. Four peptides were thus designed on the

https://doi.org/10.1021/acschemneuro.3c00208
ACS Chem. Neurosci. XXXX, XXX, XXX−XXX

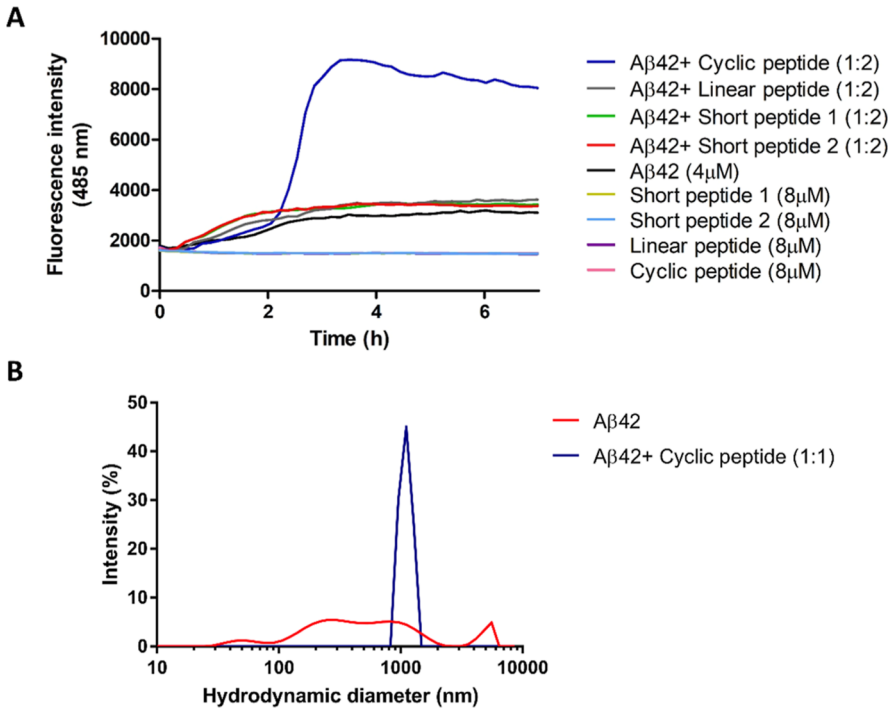

Figure 2. Cyclic peptide promotes the formation of Aβ42 aggregates. (A) Aβ42 aggregation was monitored using a ThT assay. Aβ42 was incubated alone (black curve) or separately, at 1:2 Aβ42/peptide molar ratio, with the cyclic peptide (blue curve), the linear peptide (gray curve), short peptide 1 (green curve), and short peptide 2 (red curve). The remaining curves represent the different peptides incubated alone, which did not form detectable aggregates. For these experiments, the peptides were dissolved in phosphate buffer (20 mM sodium phosphate, pH 7.4, 150 mM NaCl) supplemented with 10 μM ThT. The samples were incubated for 7 h at 37 °C with continuous shaking. (B) DLS measurements. Aβ42 (red) and an Aβ42 + peptide mixture (1:1 Aβ42/peptide molar ratio; blue) were incubated for 18 h at 37 °C before measurements. Each curve represents an average intensity size distribution of the samples (n = 12).

basis of the β-hairpin region within the APPI domain, as follows: two short 8-mer peptides, each representing a different half of the β-hairpin sequence; a third, linear, 18-mer peptide derived from the full β-hairpin sequence; and a fourth, 20-mer, cyclic peptide that was the same as the third peptide but with two cysteine residues added at the sequence ends to form the cyclic structure (Figure 1). We therefore started this study with a determination of the secondary structure of these four peptides [using spectroscopic techniques, including circular dichroism (CD) and tryptophan fluorescence measurements]. Thereafter, we demonstrated that the cyclic peptide enhanced the formation of high-molecular-weight Aβ42 aggregates [using CD and transmission electron microscopy (TEM) experiments]. Finally, we showed that the cyclic peptide reduced Aβ42-mediated toxicity in SH-SY5Y cells.

We were then in a position to leverage the peptides that had been designed and tested to address the ultimate aim of the study—to throw light on the mechanism of Aβ42 neurotoxicity, currently believed to be driven by interactions between Aβ42 oligomers and membrane phospholipids. To this end, we used a model system comprising artificial phospholipid membranes mimicking plasma and mitochondrial membranes,[40−42] as has been done previously. For example, Press-Sandler and Miller used a model system of 1,2-dioleoyl-*sn*-glycero3-phosphocholine (DOPC) lipids, which mimic plasma membrane phospholipids, to follow the behavior of Aβ42 dimers upon insertion into DOPC lipid vesicles. They found that nucleation of the Aβ42 dimers (exposing a hydrophobic core) was followed by their rearrangement as β-hairpin strands and hence a decrease in the thickness of the DOPC bilayer membrane.[41] In a similar vein, other studies demonstrated the interaction of Aβ42 with DOPC vesicles containing cardiolipin (CL) lipids, which, in nature, are present almost exclusively in the inner mitochondrial membrane and play a significant role in amyloid−membrane interactions.[22,40,43] The above studies concluded that the interaction of Aβ42 with hydrophobic membrane phospholipids facilitates the self-assembly of Aβ42 monomers into low-molecular-weight oligomers that can be internalized into cells.[24,44]

In this paper, we show that the interaction of the above-described cyclic peptide with Aβ42 enhanced the formation of high-molecular-weight Aβ42 aggregates and that in the presence of the cyclic peptide, the interactions of Aβ42 with both artificial membrane phospholipids and intact plasma and mitochondria membranes were weakened. Importantly, the cyclic peptide also exhibited an inhibitory effect against Aβ42-mediated mitochondrial membrane depolarization and reduced Aβ42-mediated apoptosis and death in SH-SY5Y cells. Taken together, these findings demonstrate the ability of the cyclic peptide to reduce the neurotoxicity of Aβ42 aggregates.

RESULTS AND DISCUSSION

Design of APPI Fragments with a β-Sheet Fold (Short Peptides). To examine the effects of APPI fragments on Aβ42 aggregation, we designed four short synthetic peptide fragments derived from the β-hairpin region of the APPI (Figure 1A). This region consists of two β-strands that also serve as the hydrophobic core within the APPI scaffold.[45] The two β-strand sequences, designated short peptides 1 and 2 (Figure 1B), were synthesized first, and then—to enable testing of the entire

https://doi.org/10.1021/acschemneuro.3c00208
ACS Chem. Neurosci. XXXX, XXX, XXX−XXX

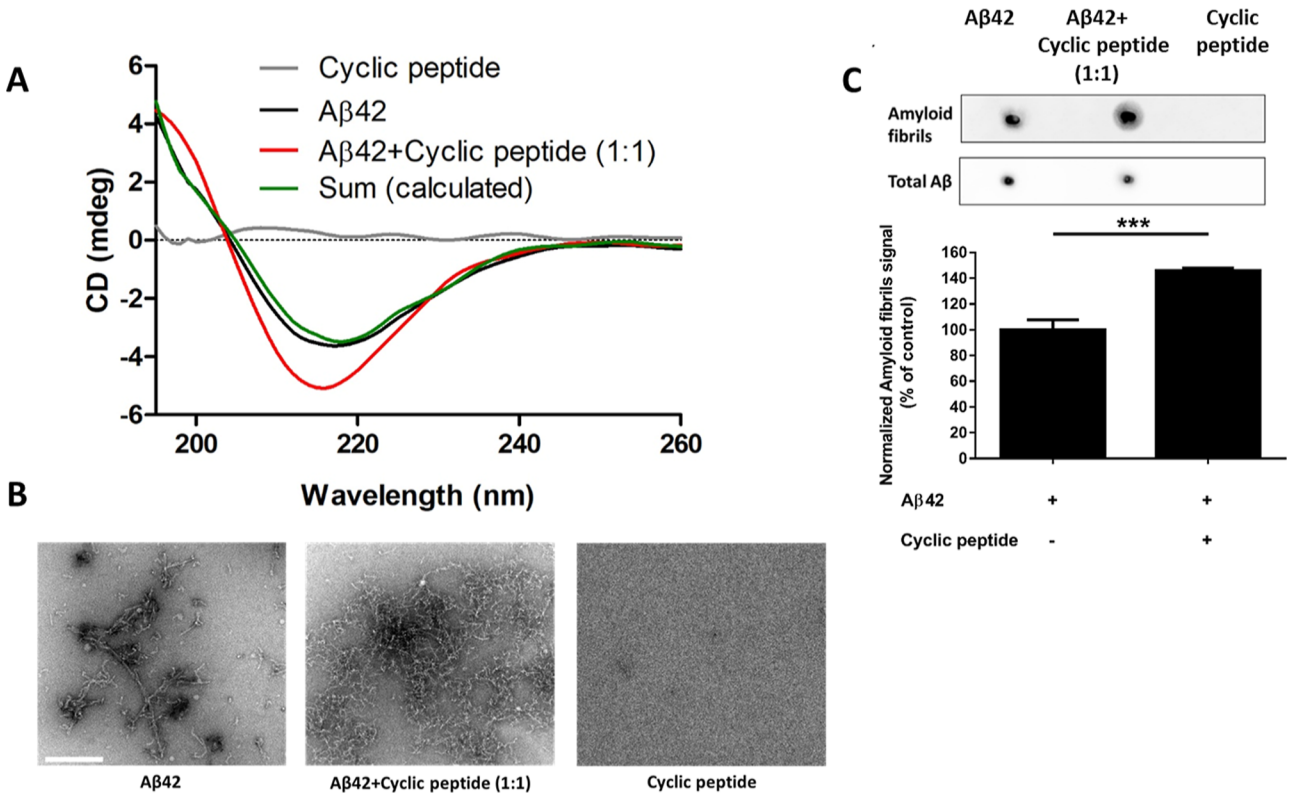

Figure 3. Enhancement by the cyclic peptide of the β-sheet and fibril contents in Aβ42 aggregates. (A) CD spectra of Aβ42, in the absence (black) or presence of the cyclic peptide (red), and of the cyclic peptide alone (light gray) after 18 h of incubation. The calculated sum of the spectra for Aβ42 and the cyclic peptide is shown in green. (B) TEM images of the CD samples: Aβ42 (left panel), Aβ42 incubated with cyclic peptide at 1:1 Aβ42/peptide molar ratio (middle panel), and cyclic peptide (right panel). Scale bar for all panels—200 nm. (C) Quantification of fibril formation as detected by an anti-Aβ fibril antibody by using dot blot analysis. Statistical analysis (n = 3) was performed by an unpaired Student's t-test. ***, P < 0.005.

hydrophobic structure derived from the APPI—two larger peptides, one linear and the other cyclic, containing the full β-hairpin structure were also synthesized (Figure 1C,D). The linear peptide was chosen on the basis of the assumption that it would spontaneously fold to form a β-hairpin structure, as in the structure of the full-length APPI. The cyclic peptide was similar to the linear peptide, except for the addition of one cysteine residue at its N-terminus and one at its C-terminus. The cysteines were added to generate a disulfide bridge between the residues that flank the peptide, thus mimicking the β-hairpin structure in the APPI.[46] For this reason, the internal cysteine in short peptide 2 that was used to generate the linear and the cyclic peptides was replaced with serine so that no undesired disulfide bonds would be formed spontaneously between the peptide monomers. In addition, to mimic the native protein sequences, the N- and C-termini of all four peptides were acetylated and amidated, respectively.

Cyclic Peptide Exhibits a Predominantly β-Sheet Secondary Structure. Mass spectrometry analysis confirmed the formation of a disulfide bridge between the N- and C-termini of the cyclic peptide and the correct molecular weights for all peptides (Figure S1). For example, the predicted molecular weights of the linear peptide and the oxidized cyclic peptide were 2254.51 and 2458.78 Da, respectively, and the experimentally obtained molecular weights were 2254.2 and 2458.2 Da, respectively. The purity of these peptides was confirmed by HPLC analysis (Figure S2). In addition, to examine the secondary structure of the peptides (reconstituted from powder with the appropriate buffer) and to follow their conformation over time, CD (Figure S3A) and tryptophan fluorescence emission spectra were obtained. The CD signature of the cyclic peptide revealed a random coil at 197 nm and a sharp peak at 218 nm, which indicates a β-sheet secondary structure. In contrast, the linear peptide and the two short peptides demonstrated random coil signatures (i.e., a peak at 197 nm), which may explain their inability to self-assemble spontaneously into an oligomeric β-sheet structure. It is likely that the moderate peak at 218 nm for short peptide 1 was due to the presence of charged amino acids (arginine and aspartic acid), which probably facilitated its arrangement into an anti-parallel structure.[47] Notably, there was no change in the secondary structure of the peptides over 24 h, which indicates that these structures are stable. In the tryptophan fluorescence emission spectra, a blue spectral shift of approximately 10 nm for the cyclic vs the linear peptide and short peptide 1 (Figure S3B) probably derives from differences in the tryptophan environment due to the formation of a β-sheet structure for the cyclic peptide,[48] but not for the linear peptide or for short peptide 1, as was also indicated by the CD spectra (Figure S3A). Short peptide 2 was not tested in this assay, because it does not have a tryptophan residue in its sequence.

Cyclic Peptide Significantly Increases the Formation of Aβ42 Aggregates. Incubation of the Aβ42 monomer with the cyclic peptide at a 1:2 molar ratio resulted in significantly enhanced Aβ42 aggregation, as indicated by an increase in the fluorescence intensity of the thioflavin T (ThT) signal relative to Aβ42 alone, which showed a typical aggregation pattern[49]

https://doi.org/10.1021/acschemneuro.3c00208
ACS Chem. Neurosci. XXXX, XXX, XXX−XXX

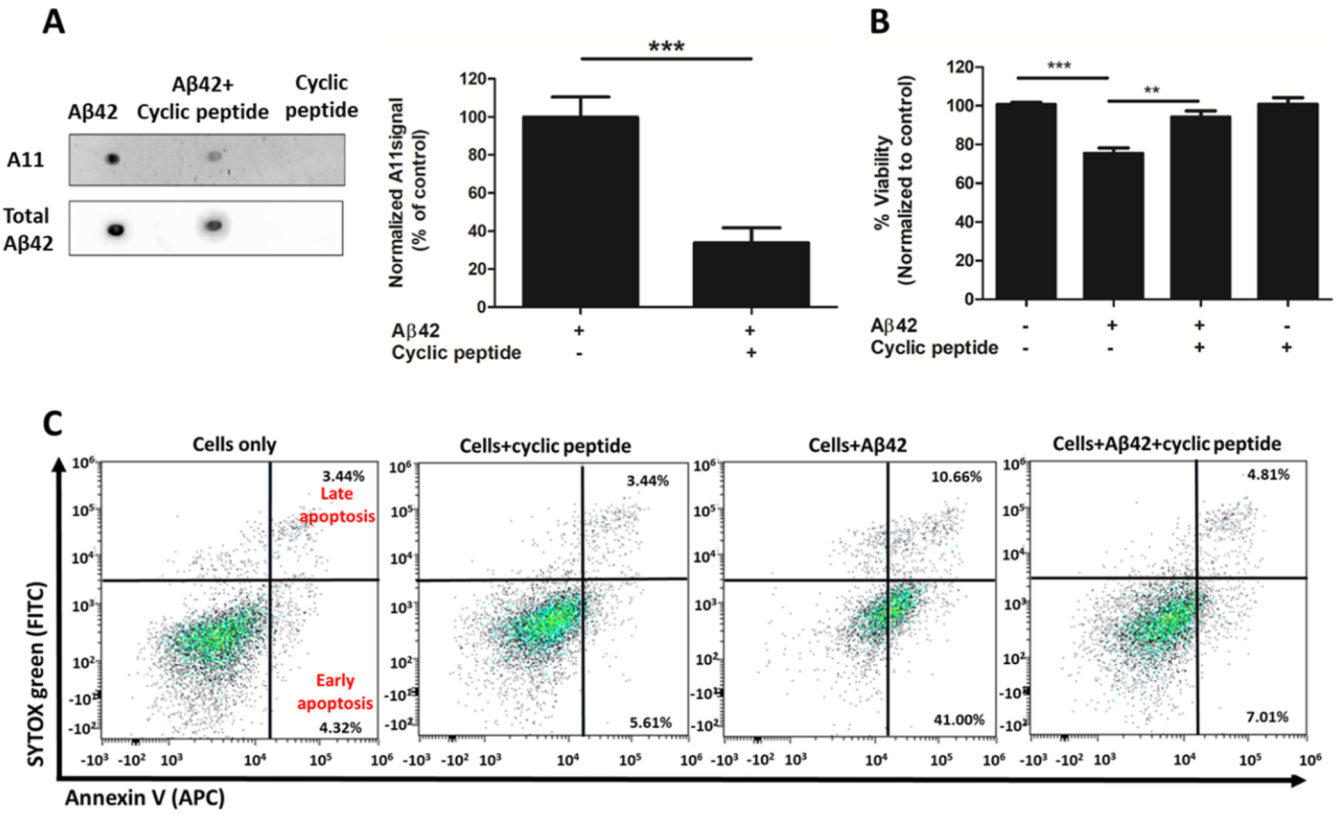

Figure 4. Cyclic peptide reduces both the quantity of toxic Aβ42 oligomers and their toxicity to SH-SY5Y cells. (A) Dot blot analysis and quantification of the A11 antibody, which detects toxic Aβ oligomers. (B) Crystal violet staining of cells treated with Aβ42 (15 μM), in the absence or presence of 15 μM cyclic peptide, or cyclic peptide alone after 48 h of incubation. Statistical analysis (n = 3) was performed by unpaired Student's t-test. **, $P < 0.01$; ***, $P < 0.001$. (C) Detection of apoptosis by FACS analysis. Annexin-V and SYTOX Green staining were used to detect the apoptosis stages of SH-SY5Y cells. Untreated cells served as a negative control.

(Figure 2A). An additional experiment at an Aβ42/cyclic peptide molar ratio of 1:1 also showed increased formation of Aβ42 aggregates (although to a lesser degree), providing an indication of the potency of the cyclic peptide (Figure S4). Addition of the linear and short peptides to Aβ42 had only a minor effect on the aggregation process, as was reflected by minor changes in the fluorescence intensity of the ThT signal. Finally, there was no signal for aggregation when the peptides were incubated alone, which indicates that there was no formation of β-sheet aggregates in the absence of Aβ42.

The significant contribution of the cyclic peptide to Aβ42 aggregation was validated by dynamic light scattering (DLS) (Figure 2B). When Aβ42 was allowed to aggregate alone, the DLS measurements showed a wide size distribution of the resulting aggregates, but incubation of Aβ42 with the cyclic peptide produced a homogenous population with larger Aβ42 aggregates vs untreated Aβ42. The cyclic peptide did not self-aggregate at the working concentrations (Figures 2A and 3A,B), and it was therefore not included in the DLS experiment. Based on these observations showing the contribution of the cyclic peptide (but not the other three peptides) to Aβ42 aggregation, we continued this study with the cyclic peptide alone.

Cyclic Peptide Promotes an Increase in the β-Sheet and Fibril Contents of Aβ42 Aggregates. Our next step was to examine the structural characteristics of the Aβ42 aggregates by using spectroscopic methods. First, CD measurements were performed to follow the structural changes that Aβ42 undergoes when treated with the cyclic peptide at a 1:1 Aβ42/peptide molar ratio (Figure 3A). Although both untreated and treated Aβ42 showed a well-ordered β-sheet secondary structure signature with a typical peak at 216 nm, as reported in previous studies,[50−52] a significant increase in the β-sheet content of the treated Aβ42 was observed. Since the cyclic peptide alone did not generate any detectable CD signal, the enhancement of the CD signal may be attributed to the interaction of Aβ42 with the cyclic peptide. The calculated sum of the CD ellipticity values of the spectra of the cyclic peptide and Aβ42 differed from the spectrum obtained for the Aβ42/cyclic peptide mixture, indicating the existence of interactions between Aβ42 and the cyclic peptide (a method of analysis described in previous reports).[53−55] Importantly, the formation of the β-sheet structure in freshly dissolved Aβ42 in the presence of the cyclic peptide was detected immediately upon addition of the cyclic peptide to the Aβ42 solution (i.e., at incubation time 0), whereas Aβ42 alone showed a predominantly random structure with a typical minimum at 197 nm (Figure S5A).[50,51] Here again, the calculated sum of the individual spectra of Aβ42 and the cyclic peptide (when measured separately) differed from the CD spectrum that was obtained for the mixture, indicating that Aβ42-cyclic peptide interactions occurred immediately upon mixing the peptides. Moreover, the signal of the anti-Aβ42 fibril antibody in the mixture of Aβ42 with the cyclic peptide significantly increased in comparison to untreated Aβ42, suggesting that the cyclic peptide rapidly enhanced the formation of high-molecular-weight Aβ42 aggregates (Figure S5B).

https://doi.org/10.1021/acschemneuro.3c00208
ACS Chem. Neurosci. XXXX, XXX, XXX−XXX

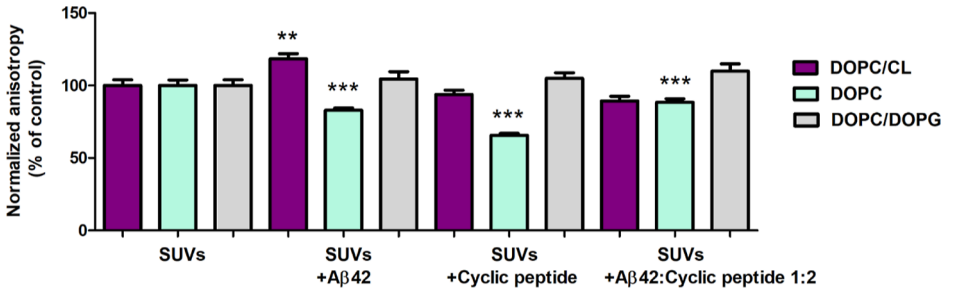

Figure 5. Cyclic peptide disrupts the interactions between Aβ42 and artificial phospholipid membranes. DPH fluorescence anisotropy of DOPC (light green bars), DOPC/CL (90:10; purple bars), and DOPC/DOPG (80:20; light gray bars) vesicles after 48 h of incubation without or with Aβ42, cyclic peptide, or a 1:2 mixture of Aβ42/cyclic peptide, as determined with an FL920 spectrofluorometer. Statistical analysis (n = 5) was performed by an unpaired Student's t-test. **, $P < 0.01$; ***, $P < 0.001$.

To confirm the enhancement in Aβ42 aggregation upon treatment with the cyclic peptide, TEM imaging was performed on the CD samples (i.e., 18 h post-incubation). Consistent with the structural results (Figures 2A and 3A) and with previous studies,[51,56] TEM images demonstrated the formation of elongated fibrils for untreated Aβ42 (Figure 3B), but in low quantities. TEM images for the Aβ42 treated with the cyclic peptide revealed more fibrils, and those species appeared to be shorter and more branched, whereas no fibrils were detected in the sample containing the cyclic peptide alone. Upon incubation of Aβ42 with the cyclic peptide for 24 h, the percentage of Aβ42 fibrils detected by an anti-amyloid fibril antibody was approximately 45% higher than that in the absence of the cyclic peptide, again suggesting enhanced production of fibrillar Aβ42 aggregates upon treatment with the cyclic peptide (Figure 3C). The cyclic peptide alone did not produce any detectable signal in this assay.

Enhancement of the Aβ42 Fibrillar Structure by the Cyclic Peptide Abolishes Toxicity in SH-SY5Y Cells. There is increasing evidence that well-ordered Aβ42 fibrils are less toxic than low-molecular-weight oligomers.[25−27] For example, Pan et al. showed a significant reduction (of 39.8%) in cell viability of primary murine microglial cells treated with Aβ42 oligomers vs cells treated with fibrillar Aβ42, which did not affect cell viability.[57] Similarly, Balducci et al. reported that injection of synthetic Aβ42 oligomers into the brains of mice resulted in long-term memory impairment, whereas mature Aβ42 fibrils had no effect.[27] Based on such reports, we sought to test whether the cyclic peptide could reduce Aβ42-mediated cytotoxicity. We therefore examined the toxicity of Aβ42 aggregates by using a conformation-specific antibody, namely, the A11 antibody, which recognizes toxic oligomers.[58] As shown in Figure 4A, the cyclic peptide reduced, by ∼70%, the quantity of toxic soluble oligomers identified by the A11 antibody. These results indicate that the cyclic peptide alters the Aβ42 oligomerization pathway such that Aβ42 forms more fibrils (previously shown to be less toxic,[59] Figure 3C) and fewer soluble oligomers (previously shown to be more toxic[58]), as shown in Figure 4A.

To validate these results in cells, we performed cell-based assays to study cell viability and apoptosis in response to treatment with Aβ42, the cyclic peptide, or an Aβ42-cyclic peptide mixture. Crystal violet staining of live cells revealed decreased cell toxicity in SH-SY5Y neuroblastoma cells treated with a mixture of Aβ42 and cyclic peptide (94% viability) vs cells treated with preformed Aβ42 aggregates (75% viability) (Figure 4B). The staining also showed that treatment with the cyclic peptide alone did not affect cell viability (100% viability) in comparison to untreated cells.

We also investigated the ability of the cyclic peptide to prevent apoptosis since it has previously been shown that Aβ42 causes cell death by increasing cellular calcium levels and causing mitochondrial damage, which leads to an apoptotic cascade.[40,60−63] To this end, we followed the percentages of cells treated with Aβ42, the cyclic peptide, or an Aβ42-cyclic peptide mixture at each apoptotic stage (early or late apoptosis) by using annexin-V/SYTOX Green labeling and flow cytometry analysis (Figure 4C). Cells stained with annexin-V but not with SYTOX Green were classified as early apoptotic cells, and cells that were positive for both SYTOX Green and annexin-V staining were classified as late apoptotic cells. We found that 41 and 10.66% of the SH-SY5Y cells that had been exposed to Aβ42 aggregates were at the early and late apoptosis stages, respectively. In contrast, the cells that had been treated with Aβ42 in the presence of the cyclic peptide (i.e., Aβ42-cyclic peptide aggregates) showed a significant reduction in cell toxicity, namely, only 7.01 and 4.81% of the cells were at early and late apoptosis stages, respectively. Treatment with the cyclic peptide alone did not cause any toxic effect (i.e., only 5.61% of cells were at the early apoptosis stage), similar to the untreated control group (4.32% of cells). Moreover, the percentage of late apoptotic cells in response to treatment with either the cyclic peptide or the preformed Aβ42-cyclic peptide aggregates was similar to that of untreated control cells (i.e., 3.44, 4.81, and 3.44%, respectively), suggesting that the cyclic peptide rescued the cells from Aβ42-mediated apoptosis. These observations are in agreement with previous studies that showed an increased rate of apoptosis in cells treated with Aβ42. Taken together, these findings show that treatment with the cyclic peptide suppressed the Aβ42-mediated apoptosis and death in SH-SY5Y cells. Moreover, they indicate the potency of the cyclic peptide as an inhibitor of Aβ42-mediated toxicity without it itself being toxic to the cells.

Interactions between Aβ42 and Biomimetic Phospholipid Membranes Are Disrupted in the Presence of the Cyclic Peptide. It has been shown that Aβ42-mediated cell cytotoxicity may be a result of the interactions of Aβ42 with the plasma and/or inner mitochondrial membranes, which lead to fluidity and permeability changes in these membranes.[40,64,65] To shed light on the mechanism of inhibition of Aβ42-mediated cell cytotoxicity by the cyclic peptide (on the molecular level), we sought to examine its effect on the interaction of Aβ42 with small unilamellar vesicles (SUVs) composed of zwitterionic DOPC or DOPC mixed

https://doi.org/10.1021/acschemneuro.3c00208
ACS Chem. Neurosci. XXXX, XXX, XXX−XXX

with negatively charged CL, which mimic the plasma and the inner mitochondrial membranes, respectively. The choice of SUVs, rather than large unilamellar vesicles, was based on previous studies showing that SUVs bind more efficiently to Aβ42 and enhance the aggregation process due to their higher curvature. The curvature of the SUVs facilitates hydrophobic clefts within the bilayer, which serve as binding sites to Aβ42 and thus promote its aggregation.[66] Moreover, the above artificial membrane compositions (i.e., DOPC and DOPC/CL SUVs) are commonly used as models in studies of neuronal cells.[41,67,68] Specifically, previous studies have characterized the effect of Aβ42 on artificial membranes made up of these lipid compositions.[40,43]

To monitor the changes in the fluidity of the artificial membranes, we used fluorescence anisotropy with the spin probe 1,6-diphenylhexatriene (DPH) intercalated within the artificial membranes. The experiments showed that 24 h of incubation of the SUV system (DOPC or DOPC/CL) with Aβ42, the cyclic peptide, or a mixture of the two in a 1:2 molar ratio resulted in only minor changes in vesicle fluidity (Figure S6). However, after 48 h of incubation, DOPC/CL SUVs treated with Aβ42 exhibited an increased anisotropy signal, indicating the interaction of Aβ42 with the lipids and an increase in vesicle rigidity (Figure 5). Similar changes in fluidity were previously suggested to be a result of interactions between Aβ42 oligomers and lipids.[43,69] However, the anisotropy signal for the DOPC/CL vesicles treated with a mixture of Aβ42 and the cyclic peptide was similar to that of the untreated DOPC/CL, indicating that the cyclic peptide preserved the fluidity of the SUVs. The results for the treatment of the vesicles with the cyclic peptide alone indicated that the cyclic peptide had no effect on the fluidity of the DOPC/CL SUVs. Based on these observations and our other experiments (Figures 3 and 4A), we propose that the cyclic peptide interferes with the interaction of Aβ42 with the DOPC/CL SUVs by promoting a decrease in the quantity of Aβ42 oligomers.

Control experiments were conducted with SUVs containing both DOPC and 1,2-dioleoyl-*sn*-glycero-3-phospho-(1′-rac-glycerol) (DOPG) and having the same charge as the DOPC/CL SUVs. Unlike the DOPC/CL SUVs, there was no change in the fluidity of the DOPC/DOPG SUVs upon treatment with Aβ42, suggesting that the effect of Aβ42 on membrane fluidity was specific to the type of lipids (CL in this case) and was not dependent on charge of the SUVs, which is identical for DOPC/CL and DOPC/DOPG vesicles. On the other hand, for DOPC vesicles mimicking the cell membrane, the 48 h anisotropy signal decreased (which means an increase in membrane fluidity) in the presence of Aβ42 or the cyclic peptide. In contrast, the anisotropy signal of DOPC SUVs treated with the mixture of Aβ42 and the cyclic peptide was the same as that for untreated DOPC SUVs, indicating that, like in the case of DOPC/CL, the cyclic peptide reduced the Aβ42 interactions with DOPC. These results are also in agreement with a previous study that showed accumulation of Aβ42 oligomers within the bilayer of DOPC lipid vesicles.[70,71] Our results suggest that the enhancement of Aβ42 aggregation (both kinetically and quantitatively) in the presence of the cyclic peptide (as shown in Figure S4) may change the way in which the membranes interact with Aβ42 and thereby inhibit the disruption of the membranes by Aβ42.

Cyclic Peptide Suppresses the Mitochondrial Membrane Depolarization Potential Mediated by Aβ42 in SH-SY5Y Cells. In light of the anisotropy results showing that the cyclic peptide reduced the interactions of Aβ42 with the biomimetic mitochondrial membrane (DOPC/CL), we sought to examine the effect of different treatments on the mitochondrial membrane potential of intact SH-SY5Y cells. The changes in mitochondrial polarization were followed to assess mitochondrial damage resulting from exposure to toxic Aβ42 oligomers and inhibition of this mitochondrial damage by the cyclic peptide. As shown in Figure 6, upon addition of preformed low-molecular weight Aβ42 oligomers to the cells, there was a ∼15% reduction in the mitochondrial membrane potential (leading to mitochondrial damage[40,72]) in comparison to untreated cells. This reduction was abolished in cells treated with Aβ42 high-molecular-weight fibrils that were formed in the presence of cyclic peptide (Figure 3A). We note that treatment with the cyclic peptide alone did not affect the membrane potential. Taken together, the results of our experiments indicate that the cyclic peptide modulated the damage caused by Aβ42 to both mitochondrial and artificial membranes.

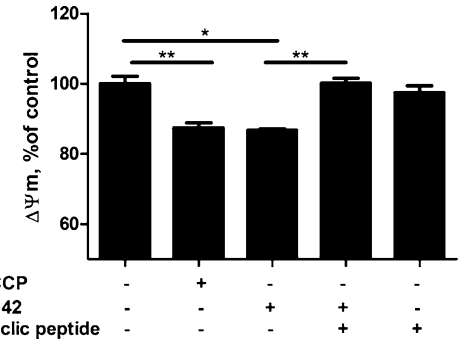

Figure 6. Suppression of Aβ42-mediated mitochondrial membrane depolarization potential ($\Delta\Psi$m) by the cyclic peptide in SH-SY5Y cells. Cells were incubated with 15 μM of Aβ42 aggregates pre-incubated in the absence and presence of the cyclic peptide at a molar ratio of 1:1 for 48 h, after which the tetramethylrhodamine, ethyl ester (TMRE) mitochondrial membrane potential assay was performed. Carbonyl cyanide-*p*-trifluoromethoxyphenylhydrazone (FCCP) served as the control for depolarization of the mitochondrial membrane potential. Statistical analysis (n = 5) was performed by an unpaired Student's *t*-test *, $P < 0.5$; **, $P < 0.01$; ***, $P < 0.001$.

Cyclic Peptide Inhibits the Interactions of Aβ42 with SH-SY5Y Cells. Previous studies have shown that in addition to interactions between intracellular Aβ42 and mitochondrial membrane, extracellular Aβ42 species also interact with plasma cell membranes and are internalized into cells via multiple uptake mechanisms.[40,73] To test the effect of the cyclic peptide on the interactions between Aβ42 and the cell membrane, we performed live imaging on SH-SY5Y cells using confocal microscopy. We observed that cells treated with HiLyte Fluor 488-Aβ42 aggregates showed a strong fluorescence signal, which was localized on the cell membrane, indicating strong interactions between Aβ42 and the cell surface (Figure 7, upper panels). However, treating the cells with a mixture of cyclic peptide and HiLyte 488-Aβ42 at molar ratios of 1:1 and 1:2 led to a decrease in the fluorescence signal, suggesting that the cyclic peptide reduced the interaction between Aβ42 and the cell membrane (Figure 7, middle and lower panels).

Proposed Mechanism for Cyclic-Peptide-Induced Neuroprotection against Toxic Aβ42 Oligomers. On

https://doi.org/10.1021/acschemneuro.3c00208
ACS Chem. Neurosci. XXXX, XXX, XXX−XXX

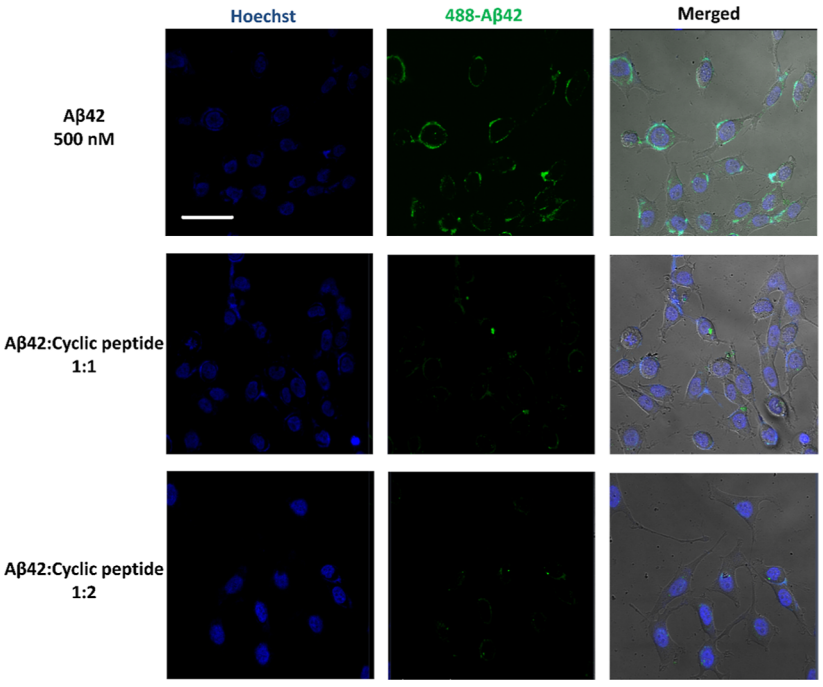

Figure 7. Inhibition of the interactions between Aβ42 and SH-SY5Y cells by the cyclic peptide. Confocal microscopy imaging of living SH-SY5Y cells. Cells were incubated with preformed aggregates of either 500 nM HiLyte 488-Aβ42 (upper panels) or with a mixture of the cyclic peptide and HiLyte 488-Aβ42 at molar ratios of 1:1 and 1:2 (HiLyte 488-Aβ42/cyclic peptide) (middle and lower panels, respectively) for 18 h. Hoechst 33342 was used for nuclear staining. Live imaging was performed using ZEISS LSM 880 microscopy, and the images were obtained with a ×40 objective. Scale bar, 50 μm.

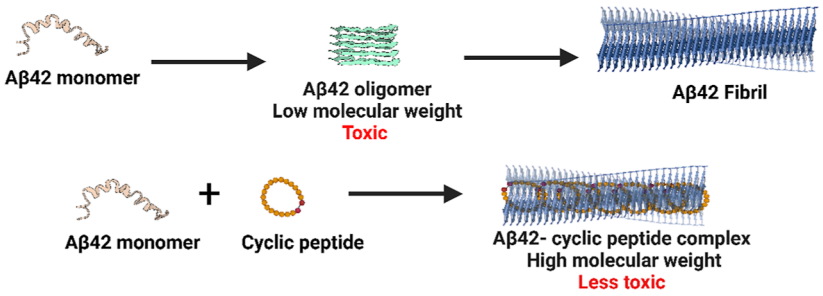

Figure 8. Proposed mechanism of the Aβ42 aggregation process in the presence of the cyclic peptide. Upper panel: Aβ42 monomers (beige; PDB: 1Z0Q) assemble into toxic oligomeric species (light green; PDB: 2BEG), which subsequently form mature fibrils (blue; PDB: 2MXU). Lower panel: Cyclic peptide (orange) binds to Aβ42, enhancing its assembly into high-molecular-weight fibrils, which are less toxic than the Aβ42 oligomeric species. This graphical illustration was created with BioRender.com.

the basis of our experimental data, Figure 8 illustrates the proposed mechanism of the effect of the cyclic peptide on Aβ42 aggregation and hence on neurotoxicity. The upper panel illustrates the structural conversion of Aβ42 monomers into low-molecular-weight oligomers, which are considered to be the most toxic species in AD development and progression.[74] The toxicity may be attributed to the interactions of Aβ42 oligomers with cell and mitochondrial membranes and subsequent destabilization of the membranes. The lower panel in Figure 8 suggests that co-incubation of Aβ42 with our cyclic peptide enhances—both kinetically and quantitatively—the formation of mature Aβ42 fibrils from intermediate, low-molecular-weight toxic oligomeric Aβ42 species and thus induces a neuroprotective effect. Our findings thus demonstrate the potential of the cyclic peptide to serve as a therapeutic agent against Aβ42-mediated neurotoxicity.

CONCLUSIONS

Previous studies (both experimental studies and those using computational modeling) have shown that Aβ42 interacts with lipid membranes,[40,41,44] thereby disrupting membrane integrity and hence exerting a neurotoxic effect. There is mounting evidence that Aβ42 can disrupt membrane integrity by several mechanisms—including, but not limited to, direct binding to phospholipids—but the molecular mechanisms underlying the membrane disruption remain to be elucidated. Against this background, we set out to apply a rational design method for investigating Aβ42−phospholipids interactions as a means to better understand the mechanisms controlling the mitochondrial and cell membrane disruptions caused by Aβ42. We showed that the cyclic peptide synthesized in this study reduced the neurotoxicity of Aβ42 aggregates by enhancing the formation of high-molecular-weight Aβ42 aggregates, modulating the interactions of Aβ42 with both artificial membrane phospholipids and intact plasma and mitochondria mem-

https://doi.org/10.1021/acschemneuro.3c00208
ACS Chem. Neurosci. XXXX, XXX, XXX−XXX

branes, and endowing protective effects against Aβ42-mediated cytotoxicity (manifested in apoptosis and mitochondrial membrane depolarization). This study thus established the basis for the rational design of a peptide inhibitor for Aβ42 toxicity. Further study should include high-throughput screening for inhibitors as well as enhancers of Aβ42 aggregation in the presence of lipids, as recently conducted for small molecules.[75]

MATERIALS AND METHODS

Materials. 1,1,1,3,3,3-Hexafluoro-2-propanol (HFIP) and 1,6-diphenyl-1,3,5-hexatriene (DPH) were purchased from Sigma-Aldrich (Rehovot, Israel). Cardiolipin (heart, bovine) sodium salt (CL), 1,2-dioleoyl-*sn*-glycero-3-phosphocholine (DOPC), 1,2-dimyristoyl-*sn*-glycero-3-phosphocholine (DMPC), and 1,2-dioleoyl-*sn*-glycero-3-phospho-(1′-rac-glycerol) (sodium salt) (DOPG) were obtained from Avanti Polar Lipids Inc. (Alabaster, AL, USA).

Peptides. Synthetic Aβ (1−42) (Aβ42) was purchased from AnaSpec (Fremont, CA, USA). Synthetic peptides, i.e., short peptide 1 (ISRWYFD), short peptide 2 (KSAPFFY), cyclic peptide (CISRWYFDVTEGKSAPFFYC), and linear peptide (ISRWYFDVTEGKSAPFFY) were synthesized by and purchased from GenScript Corporation (USA).

Cell Culture. The SH-SY5Y neuroblastoma cell line was a generous gift from Prof. Varda Shoshan-Barmatz (BGU). SH-SY5Y cells were maintained at 37 °C in a humidified incubator with aeration of 5% CO_2 in Dulbecco's modified Eagle's medium (DMEM; Biological Industries, Israel) supplemented with 10% tetracycline-free fetal bovine serum (FBS), L-glutamine (2 mM), and penicillin (100 units/mL)/streptomycin (0.1 mg/mL) (Biological Industries, Israel).

Preparation of Peptide Solutions. Aβ42 (1 mg) was dissolved in HFIP (1 mL) to a final concentration of 312 μM. For each experiment, the solvent was removed from an appropriate aliquot of dissolved Aβ42 in a rotary evaporator under vacuum at room temperature. For CD measurements, 1 mg of each APPI-derived peptide was dissolved in acetonitrile (1 mL; J.T. Baker, USA). For all other experiments, APPI-derived peptides were dissolved in DMSO (1 mL; Sigma-Aldrich, Israel). All the dissolved peptides (Aβ42 and APPI-derived peptides) were stored at −4 °C until use.

Generation of Pre-incubated Peptide Samples. In all experiments (except ThT and anisotropy experiments), Aβ42, cyclic peptide, and the peptide mixtures were mixed with phosphate buffer (20 mM sodium phosphate, pH 7.4, 150 mM NaCl) and incubated in a Thermo-shaker incubator for 18 h (500 rpm, orbital shaking) at 37 °C.

CD Measurements. For characterization of the APPI-derived peptides, the dissolved peptide was mixed with a 1:4 dilution of phosphate buffer (at a final concentration of 5 mM sodium phosphate, pH 7.4, 37.5 mM NaCl). A proper high-tension (HT) voltage (<800 V) of the CD instrument was maintained for the entire experiment for all samples. The final concentration of each peptide sample was 400 μM (except for the linear peptide, for which the concentration was reduced to 300 μM because of the high HT value that was obtained at 400 μM) in 350 μL of sample volume.

To test the effect of the cyclic peptide on Aβ42 aggregation, samples of Aβ42 (20 μM in 350 μL of 1:4 diluted phosphate buffer) were incubated in the absence or presence of 20 μM cyclic peptide. The spectrum of each sample was recorded in a range between 198 and 260 nm using a quartz cuvette with a path length of 1 mm, a scanning speed of 50 nm/min, and a data interval of 0.5 nm. The samples were scanned using a Jasco J-715 spectropolarimeter (Jasco, Japan) at time zero and 24 h post-incubation, and all the spectral scans were averaged to smooth the data curves.

The background was corrected with respect to protein-free 1:4 diluted phosphate buffer. The spectrum of the Aβ42-cyclic peptide mixture was compared with the sum of the spectra of each peptide alone at the same concentration, as previously described.[53]

TEM Imaging of Aβ42 Aggregates. Samples for TEM imaging were prepared as previously described.[51] Briefly, after pre-incubation of the peptides (Aβ42, the cyclic peptide, or a mixture of Aβ42 and the cyclic peptide), 2.5 μL aliquots of the Aβ42 samples taken from the above CD assay were deposited on carbon-coated copper 300 mesh grids. After 1 min, excess liquid was carefully blotted with filter paper, and the grid was held at ambient temperature for another minute. Uranyl acetate (2% final concentration in doubly distilled water, 5 μL) was added to each sample for 1 min, and then any excess solution was carefully removed with filter paper. Images were obtained using a Tecnai G2 12 BioTWIN (FEI, Thermo Fisher Scientific, Paisley, UK) TEM with an acceleration voltage of 120 kV (Ilse Katz Institute for Nanoscale Science & Technology). Ten fields of each sample grid were analyzed.

Tryptophan Fluorescence Assay. Short peptide 1, the cyclic peptide, or the linear peptide at a final concentration of 100 μM in phosphate buffer (20 mM sodium phosphate, pH 7.4, 0.15 M NaCl) was added to the wells of a black 96-well plate (Greiner, Sigma-Aldrich, Israel). The fluorescence emission spectrum of tryptophan was monitored using a Tecan Infinite M1000 plate reader (Männedorf, Switzerland; Cytometry and Proteomics Unit, NIBN, BGU). The excitation wavelength was 295 nm, and emission spectra were recorded in the range of 300−410 nm. Background spectra of peptide-free phosphate buffer were subtracted to achieve the final emission curves. The results are presented as the averages of three repetitions.

Detection of Aβ42 Aggregation Using the ThT Assay. Each of the APPI-derived synthetic peptides at a final concentration of 8 μM in phosphate buffer (20 mM sodium phosphate, pH 7.4, 150 mM NaCl) was added to 350 μL of stock solution of phosphate buffer supplemented with 10 μM ThT (Sigma-Aldrich, Israel) and Aβ42 at a final concentration of 4 μM. Aliquots of 100 μL of the reaction mixture were added to the peptide in a black 96-well plate (Greiner Bio-One, Germany), and ThT fluorescence was monitored at 37 °C with constant orbital shaking at 218 rpm for 7 h. ThT fluorescence was measured at 5 min intervals in a Tecan Infinite M1000 plate reader (Männedorf, Switzerland; Cytometry and Proteomics unit, NIBN, BGU). The fluorescence signals were detected using excitation and emission wavelengths of 445 and 494 nm, respectively. Data are presented as mean values of triplicates subtracted from a blank containing a mixture of the ThT reagent and phosphate buffer.

Evaluation of Aggregate Size Using DLS. DLS measurements were carried out using a Zetasizer Nano-ZS (Malvern, UK). Samples of Aβ42 (40 μM), the cyclic peptide, or a mixture of the two peptides (1:1 molar ratio; 40 μM each) were incubated in phosphate buffer (20 mM sodium phosphate, pH 7.4, 0.15 M NaCl) for 24 h at 37 °C. Samples were equilibrated for 1 min at 25 °C prior to data collection. Correlograms were collected at 173° for at least 10 runs of 10 s at 25 °C. The recorded correlograms were analyzed with the CONTIN algorithm[76] provided with the instrument software.

Characterization of Aβ42 Oligomers and Fibrils Using Immunoblotting with Structural Antibodies. Aliquots of 50 μL containing 20 μM of Aβ42 diluted in a phosphate buffer were incubated at 37 °C for 18 h in the absence or presence of 20 μM cyclic peptide, with constant orbital shaking at 500 rpm. Each sample (5 μL) was loaded onto two nitrocellulose membranes, which were then blocked with 5% skim milk (Sigma-Aldrich, Israel) in Tris-buffered saline with 0.1% Tween (TBST, Biolab, Israel), and then washed with TBST (Biolab, Israel) three times for 5 min each. Thereafter, one membrane was incubated with a rabbit anti-oligomer antibody A11, which recognizes conformational oligomeric epitopes common to amyloids[69] (Thermo Fisher, Israel), diluted at 1:1000 in PBS (Biological Industries, Israel). The other membrane was incubated with a rabbit amyloid fibril polyclonal antibody (Thermo Fisher, Israel) diluted at 1:1000 in PBS (Biological Industries, Israel) for 16 h at 4 °C. Then, a secondary HRP-linked anti-rabbit antibody (Jackson, USA) diluted at 1:3000 in 5% skim milk (Sigma-Aldrich, Israel) was added, and the chemiluminescence signals were detected using an EZ-ECL kit (Biological Industries, Israel). To confirm that equal amounts of Aβ42 were loaded in each sample, the same membrane was blocked again with 5% skim milk and incubated with a mouse anti-Aβ42 antibody (Sigma-Aldrich, Israel) diluted at 1:1000

https://doi.org/10.1021/acschemneuro.3c00208
ACS Chem. Neurosci. XXXX, XXX, XXX−XXX

in PBS, followed by incubation with a secondary HRP-linked anti-mouse antibody (Cell Signaling, USA) diluted at 1:3000. Here again, the membrane was developed, and signals were detected using the EZ-ECL kit (Biological Industries, Israel). In both immunoblotting experiments, the chemiluminescence signals were visualized with a Fusion FX imaging system (Vilber Lourmat, Germany). The image intensity was quantified using ImageJ software, and the intensity values of the oligomers detected by A11 and the fibrils detected by amyloid fibril antibody were normalized to the anti-A11 antibody and anti-Aβ fibrils signals of the untreated Aβ42 samples, respectively. The experiment was performed in triplicate, and results are presented as means ± standard deviation (SD).

Preparation of SUVs. SUVs were prepared as described previously.[77] Briefly, the lipid component, namely, DOPC, DOPC/CL (90:10), or DOPC/DOPG (80:20), for the anisotropy experiments was dissolved in a mixture of chloroform/ethanol (1:1) and then dried to constant weight under a vacuum, followed by the addition of 2 mL of sodium phosphate buffer (pH 7.4). The SUVs were then freshly prepared by probe-sonication [Vibra-Cell VCX130 ultrasonic cell disrupter (Sonics, Newtown, CT)] of the dried phospholipids for a duration of 10 min at room temperature, with 20% amplitude and 59 s on/off cycles. The final total concentration of lipids in the SUVs was 1 mM.

Fluorescence Anisotropy. The fluorescent dye DPH (Sigma-Aldrich, Israel), which becomes embedded in the membrane core and interacts with the acyl chain of SUV phospholipids,[78] was incorporated into different compositions of SUVs (DOPC, DOPC/CL, and DOPC/DOPG) by adding the dye dissolved in THF (1 mg/mL) to the vesicles in a molar ratio of 1:500 (dye/lipid). After 48 h of incubation at 30 °C, fluorescence anisotropy was determined at λ_{ex} = 360 nm and λ_{em} = 430 nm on a Fluorolog spectrofluorometer (HORIBA, Japan). Data were collected before and after addition of freshly dissolved cyclic peptide (20 μM), Aβ42 (10 μM), or a mixture of the two at a molar ratio of 1:2 (Aβ42/cyclic peptide). Anisotropy values were automatically calculated by the spectrofluorometer software using the equation

$$r = \frac{(I_{VV} - GI_{VV})}{(I_{VV} - 2GI_{VH})}, \qquad G = \frac{I_{VH}}{I_{HH}}$$

where I_{VV}—intensity with the excitation and emission polarizers mounted vertically; I_{HH}—intensity with the excitation and emission polarizers mounted horizontally; I_{HV}—intensity with the excitation polarizer horizontal and the emission polarizer vertical; I_{VH}—intensity with the excitation polarizer vertical and emission polarizer horizontal. Results are presented as means ± SD of seven replicates for each experimental condition.

Crystal Violet Staining of Living Cells. For preparing a crystal violet solution, 0.125 g of crystal violet (Sigma-Aldrich, Israel) was dissolved in 50 mL of 20% methanol. SH-SY5Y cells (10^4 cells/well in a 96-tissue culture well) were incubated for 48 h with one of the following treatments: 15 μM pre-incubated Aβ42, 15 μM cyclic peptide, or a mixture of the two peptides at a molar ratio of 1:1. The supernatant was then removed, and the plate was washed gently three times with doubly distilled water. Thereafter, 100 μL of a crystal violet solution was added to each well for 30 min. After the staining, the excess crystal violet solution was removed by three cycles of washing with doubly distilled water. Finally, the fixed crystal violet stain was dissolved with 2% SDS solution (100 μL per well), and the wells were read at a wavelength of 550 nm using a BioTek Synergy 4 microplate reader. Five repetitions for each treatment were performed. The values were normalized to the control group (untreated cells).

Flow Cytometry Analysis of Apoptotic Cells. SH-SY5Y cells (2×10^4 cells per well) were seeded in a 24-well tissue culture plate (Costar, Sigma-Aldrich, Israel) and incubated for 48 h with 20 μM preformed Aβ42 aggregates in the absence or presence of 20 μM cyclic peptide. Untreated cells served as a negative control. Cells were then harvested from the medium and treated with an APC Annexin-V/SYTOX kit (Invitrogen, Carlsbad, CA) according to the manufacturer's protocol. The cells were analyzed using Sony SP6800 Spectral Analyzer (Japan; Cytometry and Proteomics unit, NIBN, BGU).

Mitochondrial Membrane Depolarization Potential Measurements. SH-SY5Y cells (1×10^4 cells per well) were seeded in a black-clear bottomed 96-well plate (Greiner, Sigma-Aldrich, Israel). On the next day, cells were treated for 24 h with samples of pre-incubated Aβ42 (15 μM), cyclic peptide (15 μM), or a 1:1 molar ratio mixture of Aβ42 and the cyclic peptide. Cells were analyzed with a TMRE-Mitochondrial Membrane Potential Assay Kit (Abcam, Cambridge, MA, USA) according to the manufacturer's protocol, with 20 μM FCCP supplied with the kit serving as the positive control. The fluorescence intensity, which indicated mitochondrial activity, was determined with a Synergy2 microplate spectrophotometer (BioTek) with a TMRE fluorescence probe with excitation and emission wavelengths of 549 and 575 nm, respectively.

Confocal Microscopy Imaging of Live Cells. To monitor the interactions of Aβ42 and the Aβ42-cyclic peptide mixture with the cell membrane, SH-SY5Y cells were seeded at 10,000 cells/well in 1 m micro-slides (Ibidi, Germany) and grown at 37 °C. After 24 h, the cells were incubated with 1 μM preformed HiLyte 488-Aβ42 aggregates in the absence or presence of either 0.5 or 1 μM cyclic peptide. After 18 h of incubation, the medium was carefully removed, and the cells were gently washed twice with PBS (Biological Industries, Israel), followed by resuspension of the cells in 200 μL of fresh DMEM. Nuclear staining was performed using Hoechst 33342 dye diluted at 1:100 (Thermo Fisher, Israel). Live fluorescence imaging was performed with a ZEISS LSM880 confocal microscope using a ×40 objective (Ilse Katz Institute for Nanoscale Science and Technology Shared Resource Facility, BGU).

Statistical Analyses. All data were analyzed statistically with GraphPad Prism, version 5.00, for Windows (La Jolla, CA, USA). Data are shown as means ± SD. Statistical significance between the control group and different treatments was determined by unpaired Student's *t*-test analysis. *P < 0.05; **P < 0.01; ***P < 0.001.

■ ASSOCIATED CONTENT

Supporting Information

The Supporting Information is available free of charge at https://pubs.acs.org/doi/10.1021/acschemneuro.3c00208.

Mass spectroscopy spectra of the designed peptides; HPLC analysis of the synthetic peptides; peptide characterization; fluorescence intensity results of ThT for measuring aggregate formation; CD spectral data and dot blot analysis for analyzing structural changes; and fluorescence anisotropy results using artificial membranes (PDF)

■ AUTHOR INFORMATION

Corresponding Author

Niv Papo − *Avram and Stella Goldstein-Goren Department of Biotechnology Engineering and the National Institute of Biotechnology in the Negev, Ben-Gurion University of the Negev, Beer-Sheva 84105, Israel;* orcid.org/0000-0002-7056-2418; Phone: 972-50-2029729; Email: papo@bgu.ac.il

Authors

Shiran Lacham-Hartman − *Avram and Stella Goldstein-Goren Department of Biotechnology Engineering and the National Institute of Biotechnology in the Negev, Ben-Gurion University of the Negev, Beer-Sheva 84105, Israel*

Reut Moshe − *Avram and Stella Goldstein-Goren Department of Biotechnology Engineering and the National Institute of Biotechnology in the Negev, Ben-Gurion University of the Negev, Beer-Sheva 84105, Israel*

https://doi.org/10.1021/acschemneuro.3c00208
ACS Chem. Neurosci. XXXX, XXX, XXX−XXX

Shani Ben-Zichri − *Department of Chemistry, Ben-Gurion University of the Negev, Beer-Sheva 84105, Israel*
Yulia Shmidov − *Department of Chemical Engineering, Ben-Gurion University of the Negev, Beer-Sheva 84105, Israel*
Ronit Bitton − *Department of Chemical Engineering and Ilse Katz Institute for Nanoscale Science &Technology, Ben-Gurion University of the Negev, Beer-Sheva 84105, Israel*
Raz Jelinek − *Department of Chemistry and Ilse Katz Institute for Nanoscale Science &Technology, Ben-Gurion University of the Negev, Beer-Sheva 84105, Israel;* orcid.org/0000-0002-0336-1384

Complete contact information is available at: https://pubs.acs.org/10.1021/acschemneuro.3c00208

Author Contributions

S.L.H., S.B.Z., and N.P. designed the research; S.L.H., R.M, S.B.Z, and Y.S. performed the research; S.L.H., R.M., S.B.Z., Y.S., R.B., R.J., and N.P. analyzed the data; S.L.H. and N.P. wrote the paper. All authors edited the manuscript and approved the final version.

Funding

This work was supported by the Worldwide Cancer Research (grant number 20−0238), the Israel Cancer Research Fund (ICRF) (grant number 846497), the Israel Science Foundation (grant number 1615/19), and the United States—Israel Binational Science Foundation (grant number 2019303) grants to N.P.

Notes

The authors declare no competing financial interest.

■ ACKNOWLEDGMENTS

The authors thank Dr. Alon Zilka for his technical assistance with FACS experiments and Dr. Alexander Upcher for assistance with the TEM operation.

■ ABBREVIATIONS

Aβ, amyloid β; Aβ42, amyloid β 1−42; AD, Alzheimer's disease; APP, amyloid precursor protein; APPI, amyloid precursor protein inhibitor; CD, circular dichroism; CL, cardiolipin; DLS, dynamic light scattering; DMEM, Dulbecco's modified Eagle's medium; DMPC, 1,2-dimyristoyl-*sn*-glycero-3-phosphocholine; DOPC, 1,2-dioleoyl-*sn*-glycero-3-phosphocholine; DOPG, 1,2-dioleoyl-*sn*-glycero-3-phospho-(1′-rac-glycerol); DPH, 1,6-diphenyl-1,3,5-hexatriene; FCCP, carbonyl cyanide-*p*-trifluoromethoxyphenylhydrazone; HFIP, 1,1,1,3,3,3-hexafluoro-2-propanol; PBS, phosphate-buffered saline; SUV, small unilamellar vesicle; TEM, transmission electron microscopy; ThT, thioflavin T

■ REFERENCES

(1) Vassar, R.; Bennett, B. D.; Babu-Khan, S.; Kahn, S.; Mendiaz, E. A.; Denis, P.; Teplow, D. B.; Ross, S.; Amarante, P.; Loeloff, R.; et al. β-Secretase Cleavage of Alzheimer's Amyloid Precursor Protein by the Transmembrane Aspartic Protease BACE. *Science* **1999**, *286*, 735−741.
(2) Murphy, M. P.; Das, P.; Nyborg, A. C.; Rochette, M. J.; Dodson, M. W.; Loosbrock, N. M.; Souder, T. M.; McLendon, C.; Merit, S. L.; Piper, S. C.; et al. Overexpression of nicastrin increases Aß production. *FASEB J.* **2003**, *17*, 1138−1140.
(3) Anandatheerthavarada, H. K.; Biswas, G.; Robin, M. A.; Avadhani, N. G. Mitochondrial targeting and a novel transmembrane arrest of Alzheimer's amyloid precursor protein impairs mitochondrial function in neuronal cells. *J. Cell Biol.* **2003**, *161*, 41−54.
(4) De Strooper, B.; Annaert, W. COMMENTARY: Proteolytic processing and cell biological functions of the amyloid precursor protein. *J. Cell Sci.* **2000**, *113*, 1857−1870.
(5) Sandbrink, R.; Masters, C. L.; Beyreuther, K. APP Gene Family Alternative Splicing Generates Functionally Related Isoformsa. *Ann. N.Y. Acad. Sci.* **1996**, *777*, 281−287.
(6) Storey, E.; Katz, M.; Brickman, Y.; Beyreuther, K.; Masters, C. L. Amyloid precursor protein of Alzheimer's disease: evidence for a stable, full-length, trans-membrane pool in primary neuronal cultures. *Eur. J. Neurosci.* **1999**, *11*, 1779−1788.
(7) Ponte, P.; DeWhitt, P. G.; Schilling, J.; Miller, J.; Hsu, D.; Greenberg, B.; Davis, K.; Wallace, W.; Lieberburg, I.; Fuller, F.; et al. A new A4 amyloid mRNA contains a domain homologous to serine proteinase inhibitors. *Nature* **1988**, *331*, 525−527.
(8) Sisodia, S. S.; Koo, E. H.; Hoffman, P. N.; Perry, G.; Price, D. L. Identification and transport of full-length amyloid precursor proteins in rat peripheral nervous system. *J. Neurosci.* **1993**, *13*, 3136−3142.
(9) Matsui, T.; Ingelsson, M.; Fukumoto, H.; Ramasamy, K.; Kowa, H.; Frosch, M. P.; Irizarry, M. C.; Hyman, B. T. Expression of APP pathway mRNAs and proteins in Alzheimer's disease. *Brain Res.* **2007**, *1161*, 116−123.
(10) Kang, J.; Muller-Hill, B. Differential splicing of Alzheimer's disease amyloid A4 precursor RNA in rat tissues: PreA4(695) mRNA is predominantly produced in rat and human brain. *Biochem. Biophys. Res. Commun.* **1990**, *166*, 1192−1200.
(11) Dahlgren, K. N.; Manelli, A. M.; Stine, W. B., Jr.; Baker, L. K.; Krafft, G. A.; LaDu, M. J. Oligomeric and fibrillar species of amyloid-beta peptides differentially affect neuronal viability. *J. Biol. Chem.* **2002**, *277*, 32046−32053.
(12) Halverson, K.; Fraser, P. E.; Kirschner, D. A.; Lansbury, P. T., Jr. Molecular determinants of amyloid deposition in Alzheimer's disease: conformational studies of synthetic .beta.-protein fragments. *Biochemistry* **1990**, *29*, 2639−2644.
(13) Festa, G.; Mallamace, F.; Sancesario, G. M.; Corsaro, C.; Mallamace, D.; Fazio, E.; Arcidiacono, L.; Garcia Sakai, V.; Senesi, R.; Preziosi, E.; et al. Aggregation States of Aβ1−40, Aβ1−42 and Aβp3−42 Amyloid Beta Peptides: A SANS Study. *Int. J. Mol. Sci.* **2019**, *20*, 4126.
(14) Lista, S.; O'Bryant, S. E.; Blennow, K.; Dubois, B.; Hugon, J.; Zetterberg, H.; Hampel, H. Biomarkers in Sporadic and Familial Alzheimer's Disease. *J. Alzheimer's Dis.* **2015**, *47*, 291−317.
(15) Andreasen, N.; Zetterberg, H. Amyloid-related biomarkers for Alzheimer's disease. *Curr. Med. Chem.* **2008**, *15*, 766−771.
(16) Lorenzo, A.; Yankner, B. A. Amyloid Fibril Toxicity in Alzheimer's Disease and Diabetesa. *Ann. N.Y. Acad. Sci.* **1996**, *777*, 89−95.
(17) Tanokashira, D.; Mamada, N.; Yamamoto, F.; Taniguchi, K.; Tamaoka, A.; Lakshmana, M. K.; Araki, W. The neurotoxicity of amyloid beta-protein oligomers is reversible in a primary neuron model. *Mol. Brain* **2017**, *10*, 4.
(18) Brouillette, J.; Caillierez, R.; Zommer, N.; Alves-Pires, C.; Benilova, I.; Blum, D.; De Strooper, B.; Buee, L. Neurotoxicity and Memory Deficits Induced by Soluble Low-Molecular-Weight Amyloid- 1-42 Oligomers Are Revealed In Vivo by Using a Novel Animal Model. *J. Neurosci.* **2012**, *32*, 7852−7861.
(19) Fuentealba, R. A.; Liu, Q.; Zhang, J.; Kanekiyo, T.; Hu, X.; Lee, J. M.; LaDu, M. J.; Bu, G. Low-Density Lipoprotein Receptor-Related Protein 1 (LRP1) Mediates Neuronal Aβ42 Uptake and Lysosomal Trafficking. *PLoS One* **2010**, *5*, No. e11884.
(20) Nagele, R. G.; D'Andrea, M. R.; Anderson, W. J.; Wang, H. Y. Intracellular accumulation of beta-amyloid(1-42) in neurons is facilitated by the alpha 7 nicotinic acetylcholine receptor in Alzheimer's disease. *Neuroscience* **2002**, *110*, 199−211.
(21) Arispe, N.; Pollard, H. B.; Rojas, E. Giant multilevel cation channels formed by Alzheimer disease amyloid beta-protein [A beta P-(1-40)] in bilayer membranes. *Proc. Natl. Acad. Sci. U.S.A.* **1993**, *90*, 10573−10577.
(22) Gobbi, M.; Re, F.; Canovi, M.; Beeg, M.; Gregori, M.; Sesana, S.; Sonnino, S.; Brogioli, D.; Musicanti, C.; Gasco, P.; et al. Lipid-

based nanoparticles with high binding affinity for amyloid-β1−42 peptide. *Biomaterials* **2010**, *31*, 6519−6529.
(23) Tahara, K.; Kim, H. D.; Jin, J. J.; Maxwell, J. A.; Li, L.; Fukuchi, K. Role of toll-like receptor signalling in A uptake and clearance. *Brain* **2006**, *129*, 3006−3019.
(24) Jin, S.; Kedia, N.; Illes-Toth, E.; Haralampiev, I.; Prisner, S.; Herrmann, A.; Wanker, E. E.; Bieschke, J. Amyloid-β(1−42) Aggregation Initiates Its Cellular Uptake and Cytotoxicity. *J. Biol. Chem.* **2016**, *291*, 19590−19606.
(25) Ahmed, M.; Davis, J.; Aucoin, D.; Sato, T.; Ahuja, S.; Aimoto, S.; Elliott, J. I.; Van Nostrand, W. E.; Smith, S. O. Structural conversion of neurotoxic amyloid-β1−42 oligomers to fibrils. *Nat. Struct. Mol. Biol.* **2010**, *17*, 561−567.
(26) Taneja, V.; Verma, M.; Vats, A. Toxic species in amyloid disorders: Oligomers or mature fibrils. *Ann. Indian Acad. Neurol.* **2015**, *18*, 138−145.
(27) Balducci, C.; Beeg, M.; Stravalaci, M.; Bastone, A.; Sclip, A.; Biasini, E.; Tapella, L.; Colombo, L.; Manzoni, C.; Borsello, T.; et al. Synthetic amyloid-beta oligomers impair long-term memory independently of cellular prion protein. *Proc. Natl. Acad. Sci. U.S.A.* **2010**, *107*, 2295−2300.
(28) Demuro, A.; Smith, M.; Parker, I. Single-channel Ca^{2+} imaging implicates Aβ1−42 amyloid pores in Alzheimer's disease pathology. *J. Cell Biol.* **2011**, *195*, 515−524.
(29) Pannuzzo, M. Beta-amyloid pore linked to controlled calcium influx into the cell: A new paradigm for Alzheimer's Disease. *Alzheimer's Dementia* **2022**, *18*, 191−196.
(30) Calvo-Rodriguez, M.; Hernando-Perez, E.; Nunez, L.; Villalobos, C. Amyloid beta Oligomers Increase ER-Mitochondria $Ca^{(2+)}$ Cross Talk in Young Hippocampal Neurons and Exacerbate Aging-Induced Intracellular $Ca^{(2+)}$ Remodeling. *Front. Cell. Neurosci.* **2019**, *13*, 22.
(31) Vadukul, D. M.; Maina, M.; Franklin, H.; Nardecchia, A.; Serpell, L. C.; Marshall, K. E. Internalisation and toxicity of amyloid-beta 1-42 are influenced by its conformation and assembly state rather than size. *FEBS Lett.* **2020**, *594*, 3490−3503.
(32) Cardoso, S. M.; Santos, S.; Swerdlow, R. H.; Oliveira, C. R. Functional mitochondria are required for amyloid beta-mediated neurotoxicity. *FASEB J.* **2001**, *15*, 1439−1441.
(33) Taylor, M.; Moore, S.; Mayes, J.; Parkin, E.; Beeg, M.; Canovi, M.; Gobbi, M.; Mann, D. M.; Allsop, D. Development of a proteolytically stable retro-inverso peptide inhibitor of beta-amyloid oligomerization as a potential novel treatment for Alzheimer's disease. *Biochemistry* **2010**, *49*, 3261−3272.
(34) Castelletto, V.; Ryumin, P.; Cramer, R.; Hamley, I. W.; Taylor, M.; Allsop, D.; Reza, M.; Ruokolainen, J.; Arnold, T.; Hermida-Merino, D.; et al. Self-Assembly and Anti-Amyloid Cytotoxicity Activity of Amyloid beta Peptide Derivatives. *Sci. Rep.* **2017**, *7*, 43637.
(35) Hochdorffer, K.; Marz-Berberich, J.; Nagel-Steger, L.; Epple, M.; Meyer-Zaika, W.; Horn, A. H.; Sticht, H.; Sinha, S.; Bitan, G.; Schrader, T. Rational Design of β-Sheet Ligands Against $A\beta_{42}$-Induced Toxicity. *J. Am. Chem. Soc.* **2011**, *133*, 4348−4358.
(36) Sun, X.; Wu, W. H.; Liu, Q.; Chen, M. S.; Yu, Y. P.; Ma, Y.; Zhao, Y. F.; Li, Y. M. Hybrid peptides attenuate cytotoxicity of beta-amyloid by inhibiting its oligomerization: implication from solvent effects. *Peptides* **2009**, *30*, 1282−1287.
(37) Gibson, T. J.; Murphy, R. M. Design of peptidyl compounds that affect beta-amyloid aggregation: importance of surface tension and context. *Biochemistry* **2005**, *44*, 8898−8907.
(38) Javed, I.; Sun, Y.; Adamcik, J.; Wang, B.; Kakinen, A.; Pilkington, E. H.; Ding, F.; Mezzenga, R.; Davis, T. P.; Ke, P. C. Cofibrillization of Pathogenic and Functional Amyloid Proteins with Gold Nanoparticles against Amyloidogenesis. *Biomacromolecules* **2017**, *18*, 4316−4322.
(39) Pilkington, E. H.; Lai, M.; Ge, X.; Stanley, W. J.; Wang, B.; Wang, M.; Kakinen, A.; Sani, M. A.; Whittaker, M. R.; Gurzov, E. N.; et al. Star Polymers Reduce Islet Amyloid Polypeptide Toxicity via Accelerated Amyloid Aggregation. *Biomacromolecules* **2017**, *18*, 4249−4260.
(40) Oren, O.; Ben Zichri, S.; Taube, R.; Jelinek, R.; Papo, N. Aβ42 Double Mutant Inhibits Aβ42-Induced Plasma and Mitochondrial Membrane Disruption in Artificial Membranes, Isolated Organs, and Intact Cells. *ACS Chem. Neurosci.* **2020**, *11*, 1027−1037.
(41) Press-Sandler, O.; Miller, Y. Molecular insights into the primary nucleation of polymorphic amyloid beta dimers in DOPC lipid bilayer membrane. *Protein Sci.* **2022**, *31*, No. e4283.
(42) Shimanouchi, T. I.; Iwamura, M.; Deguchi, S.; Kimura, Y. Fibril Growth Behavior of Amyloid β on Polymer-Based Planar Membranes: Implications for the Entanglement and Hydration of Polymers. *Appl. Sci.* **2021**, *11*, 4408.
(43) Malishev, R.; Nandi, S.; Smilowicz, D.; Bakavayev, S.; Engel, S.; Bujanover, N.; Gazit, R.; Metzler-Nolte, N.; Jelinek, R. Interactions between BIM Protein and Beta-Amyloid May Reveal a Crucial Missing Link between Alzheimer's Disease and Neuronal Cell Death. *ACS Chem. Neurosci.* **2019**, *10*, 3555−3564.
(44) Fatafta, H.; Kav, B.; Bundschuh, B. F.; Loschwitz, J.; Strodel, B. Disorder-to-order transition of the amyloid-beta peptide upon lipid binding. *Biophys. Chem.* **2022**, *280*, 106700.
(45) Salameh, M. A.; Soares, A. S.; Navaneetham, D.; Sinha, D.; Walsh, P. N.; Radisky, E. S. Determinants of affinity and proteolytic stability in interactions of Kunitz family protease inhibitors with mesotrypsin. *J. Biol. Chem.* **2010**, *285*, 36884−36896.
(46) Cho, P. Y.; Joshi, G.; Boersma, M. D.; Johnson, J. A.; Murphy, R. M. A Cyclic Peptide Mimic of the beta-Amyloid Binding Domain on Transthyretin. *ACS Chem. Neurosci.* **2015**, *6*, 778−789.
(47) Tsutsumi, M.; Otaki, J. M. Parallel and antiparallel beta-strands differ in amino acid composition and availability of short constituent sequences. *J. Chem. Inf. Model.* **2011**, *51*, 1457−1464.
(48) Kazman, P.; Absmeier, R. M.; Engelhardt, H.; Buchner, J. Dissection of the amyloid formation pathway in AL amyloidosis. *Nat. Commun.* **2021**, *12*, 6516.
(49) Biancalana, M.; Koide, S. Molecular mechanism of Thioflavin-T binding to amyloid fibrils. *Biochim. Biophys. Acta* **2010**, *1804*, 1405−1412.
(50) Dunstan, D. E.; Hamilton-Brown, P.; Asimakis, P.; Ducker, W.; Bertolini, J. Shear flow promotes amyloid- fibrilization. *Protein Eng., Des. Sel.* **2009**, *22*, 741−746.
(51) Oren, O.; Banerjee, V.; Taube, R.; Papo, N. An Aβ42 variant that inhibits intra- and extracellular amyloid aggregation and enhances cell viability. *The Biochemical journal* **2018**, *475*, 3087−3103.
(52) Granic, I.; Masman, M. F.; Kees Mulder, C.; Nijholt, I. M.; Naude, P. J.; de Haan, A.; Borbely, E.; Penke, B.; Luiten, P. G.; Eisel, U. L. LPYFDa neutralizes amyloid-beta-induced memory impairment and toxicity. *J. Alzheimer's Dis.* **2010**, *19*, 991−1005.
(53) Azoulay, Z.; Rapaport, H. The assembly state and charge of amphiphilic beta-sheet peptides affect blood clotting. *J. Mater. Chem. B* **2016**, *4*, 3859−3867.
(54) Roviello, G. N.; Vicidomini, C.; Costanzo, V.; Roviello, V. Nucleic acid binding and other biomedical properties of artificial oligolysines. *Int. J. Nanomed.* **2016**, *11*, 5897−5904.
(55) Al Adem, K.; Shanti, A.; Srivastava, A.; Homouz, D.; Thomas, S. A.; Khair, M.; Stefanini, C.; Chan, V.; Kim, T. Y.; Lee, S. Linking Alzheimer's Disease and Type 2 Diabetes: Characterization and Inhibition of Cytotoxic Aβ and IAPP Hetero-Aggregates. *Front. Mol. Biosci.* **2022**, *9*, 842582.
(56) Robert, R.; Dolezal, O.; Waddington, L.; Hattarki, M. K.; Cappai, R.; Masters, C. L.; Hudson, P. J.; Wark, K. L. Engineered antibody intervention strategies for Alzheimer's disease and related dementias by targeting amyloid and toxic oligomers. *Protein Eng., Des. Sel.* **2008**, *22*, 199−208.
(57) Pan, X. D.; Zhu, Y. G.; Lin, N.; Zhang, J.; Ye, Q. Y.; Huang, H. P.; Chen, X. C. Microglial phagocytosis induced by fibrillar beta-amyloid is attenuated by oligomeric beta-amyloid: implications for Alzheimer's disease. *Mol. Neurodegener.* **2011**, *6*, 45.
(58) Glabe, C. G. Structural classification of toxic amyloid oligomers. *J. Biol. Chem.* **2008**, *283*, 29639−29643.

https://doi.org/10.1021/acschemneuro.3c00208
ACS Chem. Neurosci. XXXX, XXX, XXX−XXX

(59) Sengupta, U.; Nilson, A. N.; Kayed, R. The Role of Amyloid-beta Oligomers in Toxicity, Propagation, and Immunotherapy. *EBioMedicine* **2016**, *6*, 42−49.
(60) Awasthi, A.; Matsunaga, Y.; Yamada, T. Amyloid-beta causes apoptosis of neuronal cells via caspase cascade, which can be prevented by amyloid-beta-derived short peptides. *Exp. Neurol.* **2005**, *196*, 282−289.
(61) Krishtal, J.; Bragina, O.; Metsla, K.; Palumaa, P.; Tougu, V. In situ fibrillizing amyloid-beta 1-42 induces neurite degeneration and apoptosis of differentiated SH-SY5Y cells. *PLoS One* **2017**, *12*, No. e0186636.
(62) Umeda, T.; Tomiyama, T.; Sakama, N.; Tanaka, S.; Lambert, M. P.; Klein, W. L.; Mori, H. Intraneuronal amyloid beta oligomers cause cell death via endoplasmic reticulum stress, endosomal/lysosomal leakage, and mitochondrial dysfunction in vivo. *J. Neurosci. Res.* **2011**, *89*, 1031−1042.
(63) Resende, R.; Ferreiro, E.; Pereira, C.; Resende de Oliveira, C. Neurotoxic effect of oligomeric and fibrillar species of amyloid-beta peptide 1-42: involvement of endoplasmic reticulum calcium release in oligomer-induced cell death. *Neuroscience* **2008**, *155*, 725−737.
(64) Bharadwaj, P.; Solomon, T.; Malajczuk, C. J.; Mancera, R. L.; Howard, M.; Arrigan, D. W. M.; Newsholme, P.; Martins, R. N. Role of the cell membrane interface in modulating production and uptake of Alzheimer's beta amyloid protein. *Biochim. Biophys. Acta, Biomembr.* **2018**, *1860*, 1639−1651.
(65) Williams, T. L.; Serpell, L. C. Membrane and surface interactions of Alzheimer's Aβ peptide - insights into the mechanism of cytotoxicity: Membrane interactions of Alzheimer's Aβ peptide. *FEBS J.* **2011**, *278*, 3905−3917.
(66) Kinoshita, M.; Kakimoto, E.; Terakawa, M. S.; Lin, Y.; Ikenoue, T.; So, M.; Sugiki, T.; Ramamoorthy, A.; Goto, Y.; Lee, Y. H. Model membrane size-dependent amyloidogenesis of Alzheimer's amyloid-beta peptides. *Phys. Chem. Chem. Phys.* **2017**, *19*, 16257−16266.
(67) Quist, A.; Doudevski, I.; Lin, H.; Azimova, R.; Ng, D.; Frangione, B.; Kagan, B.; Ghiso, J.; Lal, R. Amyloid ion channels: a common structural link for protein-misfolding disease. *Proc. Natl. Acad. Sci. U.S.A.* **2005**, *102*, 10427−10432.
(68) Jang, H.; Arce, F. T.; Ramachandran, S.; Capone, R.; Azimova, R.; Kagan, B. L.; Nussinov, R.; Lal, R. Truncated beta-amyloid peptide channels provide an alternative mechanism for Alzheimer's Disease and Down syndrome. *Proc. Natl. Acad. Sci. U.S.A.* **2010**, *107*, 6538−6543.
(69) Matveeva, E. G.; Rudolph, A.; Moll, J. R.; Thompson, R. B. Structure-selective anisotropy assay for amyloid Beta oligomers. *ACS Chem. Neurosci.* **2012**, *3*, 982−987.
(70) Hane, F.; Drolle, E.; Gaikwad, R.; Faught, E.; Leonenko, Z. Amyloid-beta aggregation on model lipid membranes: an atomic force microscopy study. *J. Alzheimer's Dis.* **2011**, *26*, 485−494.
(71) Nguyen, P. H.; Ramamoorthy, A.; Sahoo, B. R.; Zheng, J.; Faller, P.; Straub, J. E.; Dominguez, L.; Shea, J. E.; Dokholyan, N. V.; De Simone, A.; et al. Amyloid Oligomers: A Joint Experimental/Computational Perspective on Alzheimer's Disease, Parkinson's Disease, Type II Diabetes, and Amyotrophic Lateral Sclerosis. *Chem. Rev.* **2021**, *121*, 2545−2647.
(72) Cardoso, S. M.; Santana, I.; Swerdlow, R. H.; Oliveira, C. R. Mitochondria dysfunction of Alzheimer's disease cybrids enhances Aβ toxicity. *J. Neurochem.* **2004**, *89*, 1417−1426.
(73) Pedrero-Prieto, C. M.; Flores-Cuadrado, A.; Saiz-Sanchez, D.; Ubeda-Banon, I.; Frontinan-Rubio, J.; Alcain, F. J.; Mateos-Hernandez, L.; de la Fuente, J.; Duran-Prado, M.; Villar, M.; et al. Human amyloid-beta enriched extracts: evaluation of in vitro and in vivo internalization and molecular characterization. *Alzheimer's Res. Ther.* **2019**, *11*, 56.
(74) Meng, X.; Li, T.; Wang, X.; Lv, X.; Sun, Z.; Zhang, J.; Su, F.; Kang, S.; Kim, S.; An, S. S. A.; et al. Association between increased levels of amyloid-beta oligomers in plasma and episodic memory loss in Alzheimer's disease. *Alzheimer's Res. Ther.* **2019**, *11*, 89.
(75) Cox, S. J.; Lam, B.; Prasad, A.; Marietta, H. A.; Stander, N. V.; Joel, J. G.; Sahoo, B. R.; Guo, F.; Stoddard, A. K.; Ivanova, M. I.; et al. High-Throughput Screening at the Membrane Interface Reveals Inhibitors of Amyloid-β. *Biochemistry* **2020**, *59*, 2249−2258.
(76) Provencher, S. W. CONTIN: a general purpose constrained regularization program for inverting noisy linear algebraic and integral equations. *Comput. Phys. Commun.* **1982**, *27*, 229−242.
(77) Huang, C. Phosphatidylcholine vesicles. Formation and physical characteristics. *Biochemistry* **1969**, *8*, 344−352.
(78) Poojari, C.; Wilkosz, N.; Lira, R. B.; Dimova, R.; Jurkiewicz, P.; Petka, R.; Kepczynski, M.; Róg, T. Behavior of the DPH fluorescence probe in membranes perturbed by drugs. *Chem. Phys. Lipids* **2019**, *223*, 104784.

https://doi.org/10.1021/acschemneuro.3c00208
ACS Chem. Neurosci. XXXX, XXX, XXX−XXX